Self-imaging of molecules from diffraction spectra by laser-induced rescattering electrons

Junliang Xu, Zhangjin Chen, Anh-Thu Le, and C. D. Lin
J. R. Macdonald Laboratory, Physics Department, Kansas State University, Manhattan, Kansas 66506-2604, USA
(Received 8 June 2010; published 8 September 2010)

We study high-energy angle-resolved photoelectron spectra of molecules in strong fields. In an oscillating laser electric field, electrons released earlier in the pulse may return to recollide with the target ion, in a process similar to scattering by laboratory prepared electrons. If midinfrared lasers are used, we show that the images generated by the returning electrons are similar to images observed in typical gas-phase electron diffraction (GED). These spectra can be used to retrieve the positions of atoms in a molecule as in GED. Since infrared laser pulses of durations of a few femtoseconds are already available today, the study of these high-energy photoelectrons offers the opportunity of imaging the structure of transient molecules with temporal resolution of a few femtoseconds.

DOI: 10.1103/PhysRevA.82.033403 PACS number(s): 33.20.Xx, 33.60.+q, 34.80.Qb, 34.80.Bm

I. INTRODUCTION

When an object is illuminated by a plane wave, the amplitude of the far-field diffraction pattern is the Fourier transform of the object [1,2]. To get high resolution, short wavelength lights such as x rays are used for imaging the structure of molecules in the solid and liquid phases. Similarly, electrons can interact with matter to form images. There are three types of electron diffraction: the low-energy electron diffraction (LEED), the transmission high-energy electron diffraction, and the reflection high-energy electron diffraction. The latter two are major characterization techniques for surfaces. The diffraction of an object by high-energy electrons can be described based on the scattering of individual atoms, akin to x-ray diffraction and neutron diffraction. For LEED, low-energy electrons, typically from 10 to 300 eV, are used. These electrons tend to probe the valence electrons or the bonding between the atoms of the object where quantum-mechanical effects such as exchange and many-electron correlation are important. Images obtained from LEED are much more difficult to decipher; they require complicated theoretical calculations to help the interpretation.

To study the structure of isolated molecules, there are also two general approaches. To know the positions of atoms in the molecule, one uses high-energy electrons or x rays. To know the chemical bonding, one would use low-energy electrons or synchrotron light sources. Gas-phase electron diffraction (GED) [3,4] has been used for more than half a century for determining the structure of molecules. Here a well-collimated electron beam with energies in the order of hundreds keVs are employed. Molecules in the gas phase have much smaller density compared to that of molecules in the liquid or the solid phase, and gas-phase molecules are usually isotropically distributed. Using GED, the interatomic radial distributions of many molecules have been retrieved successfully. In the meantime, low-energy electrons and synchrotron light sources have been extensively used to study the structure of molecules, including biological ones. These measurements, similar to LEED, probe the valence electrons of the molecules; interpretations of their images require elaborate many-body collision theory from quantum chemistry.

Conventional x-ray and electron-diffraction tools serve well for probing accurate static structure of an object; they are not suitable for probing objects that are undergoing rapid transformations. Today molecular dynamics and some biological molecules are routinely studied using the femtosecond time scales with different spectroscopy techniques [5–9]. These low-energy measurements, however, do not give direct structural information about the atomic coordinates which are the most basic parameters of a molecule. Recently, it has been proposed that when a single molecule is exposed to a large number of photons from a short pulse of an x-ray free-electron laser (XFEL), a diffraction pattern may be captured before the molecule is destroyed if the pulse is short enough [10]. Such a proposal will be tested soon as the first x rays from the the Linac Coherent Light Source (LCLS) have been delivered since spring 2009. Still, the XFELs are large and expensive facilities; other tools would be welcome if they can serve similar purposes. Using high-energy electrons, ultrafast electron-diffraction (UED) experiments have been performed in a number of laboratories [11–13] in the last decade or so. These pulsed electrons are generated by femtosecond lasers from photocathodes and accelerated to tens or hundreds of keVs. Using UED, dynamic systems have been studied with time resolution of the order of hundreds of femtoseconds. Such a time scale is still too long for many interesting chemical reactions where fast reactions may occur within a few to tens of femtoseconds.

The XFELs and the UED both rely on taking diffraction images using high-energy photons or electrons, respectively. For dynamic imaging, the technical challenge of these approaches lies in developing light or electron sources that are intense and short enough such that diffraction images can be taken within a few femtoseconds. In this article we look for an alternative approach for dynamic imaging of a molecule using short intense infrared laser pulses [14,15]. Infrared lasers of a few femtoseconds are already available in many laboratories and universities. Thus if these laser pulses can be used to probe the structure of a molecule, then it may be possible to use infrared lasers to study the rapid structural change of a molecule. Unlike the existing ultrafast chemistry, here the goal is the ultrafast probe of the atomic coordinates of a transient molecule which are evolving with time; that is, it has the same goal as UED and XFELs.

Can infrared lasers be used to reveal the structure of a molecule? Since the wavelength of an infrared laser is much

longer than the interatomic separations in the molecule, this is not obvious. However, when a molecule is exposed to strong fields, an electron that is removed from the molecule earlier in the pulse may be driven back to recollide with its parent ion [16,17]. The scattering by these returning electrons is analogous to the scattering by a laboratory-prepared electron beam on the target. Can the "diffraction image" generated by these returning electrons be used to extract the structural information of the target? Such a potential has been proposed since the 1990s [18–20]. But careful analysis reveals two obvious obstacles: First, the electron collision occurs in the laser field, so how does the laser field modify the diffraction image [21,22]? Since laser-molecule interaction is a nonlinear process, the "diffraction image," or more precisely, the momentum distributions of the photoelectrons, cannot be accurately calculated theoretically. Without a reliable theory, the retrieval of molecular structure from the photoelectron spectra is not possible. Second, for typical Ti-sapphire lasers used in strong-field physics, the returning electrons have kinetic energies of only 15–50 eV, for peak laser intensities of $1–3 \times 10^{14}$ W/cm^2. These energies are much smaller than the hundreds of keVs used in GED. Electrons of such energies are typical of those used for probing the valence electrons. Like LEED, such diffraction images cannot be interpreted without an advanced theory, which is not available for molecules interacting with strong fields.

The optimism of our proposal for using intense infrared laser pulses for imaging molecules is due to two recent theoretical developments in strong-field rescattering physics [14,23,24]. First, by focusing only on images (or angular distributions) of high-energy above-threshold-ionization (HATI) electrons, we have shown that *field-free* electron-target ion differential cross sections (DCS) can be extracted [14,24]. These diffraction images are identical to those generated by a beam of laboratory electrons. Second, these HATI electrons are electrons backscattered by the target ion. They are scattered off from the atomic centers in the molecule, similar to GED. For such collisions, the so-called independent atom model (IAM) used in GED can be applied at low energies, say, near 100 eV or so. Such returning electrons can be easily achieved with present-day midinfrared lasers. The similarity to GED makes the interpretation of diffraction images straightforward.

An important advantage of using laser-induced electrons to generate electron-diffraction images is that it can be readily synchronized to perform typical pump-probe measurements. The pump beam may be used to orient or align molecules such that diffraction images can be taken from nonisotropically distributed molecules. This is a feature that is not yet available in standard GED today since field-free molecules can be oriented or aligned transiently only [25]. The pump laser beam, or the harmonics it generates, can also be used to initiate the dynamic evolution of a molecule. In this article, we are concerned with the probe part. In Sec. II we describe the theoretical basis that makes dynamic imaging with infrared lasers possible. In particular, the independent atom model used in GED is described. In Sec. III, we first demonstrate that the IAM can be applied to describe diffraction images for incident electron energies down to about 100 eV or less if the images are taken at large scattering angles, in contrast to the hundreds of keVs used in GED. We then illustrate how to retrieve interatomic separations for isotropically distributed molecules as well as for molecules that are aligned. We conclude this article, in Sec. IV, with a short summary and a discussion of future challenges. Atomic units are used in this article unless otherwise indicated.

II. THEORY OF DYNAMIC IMAGING WITH INFRARED LASERS

A. Independent atom model for electron-molecule collisions

In traditional gas-phase electron diffraction, a beam of electrons with energies of a few hundreds of keVs are aimed at randomly distributed molecules. The scattered electrons are measured in the forward directions. The DCS, or the diffraction images, are calculated using the IAM [26–28]. In the IAM, a molecule is modeled as a collection of its component atoms fixed in space. The potential seen by the incident electron is taken to be the sum of the individual potential from each atom. These atoms do not interact and there is no consideration of chemical bonding, nor of molecular orbitals. Let atom i be fixed at $\boldsymbol{R}_i$. The interaction potential of each atom i is represented by a short-range potential. If f_i is the complex scattering amplitude of the ith atom by the incident electron, according to the IAM, the total scattering amplitude for a molecule fixed in space is given by

$$F(k,\theta,\varphi;\Omega_L) = \sum_i f_i e^{i\boldsymbol{q}\cdot\boldsymbol{R}_i}, \tag{1}$$

where Ω_L denotes the orientationor alignment angles of the molecule, and $\boldsymbol{q} = \boldsymbol{k} - \boldsymbol{k}_0$ is the momentum transfer. The incident electron momentum $\boldsymbol{k}_0$ is taken to be along the z axis, and $\boldsymbol{k} = (k,\theta,\varphi)$ is the momentum of the scattered electrons. From Eq (1), the differential cross section is then given by

$$I_{\rm tot}(\theta,\varphi;\Omega_L) = I_A + \sum_{i\neq j} f_i f_j^* e^{i\boldsymbol{q}\cdot\boldsymbol{R}_{ij}}, \tag{2}$$

where $\boldsymbol{R}_{ij} = \boldsymbol{R}_i - \boldsymbol{R}_j$, and $I_A = \sum_i |f_i|^2$. Here I_A is an incoherent sum of scattering cross sections from all the atoms in the molecule. The second term is defined to be the molecular interference term (MIT). We can see that molecular structural information is only included in the second term, MIT. For electron scattering from a sample of randomly distributed molecules, the average of the above expression over Ω_L gives

$$\langle I_{\rm tot}\rangle(\theta) = I_A + \sum_{i\neq j} f_i f_j^* \frac{\sin(qR_{ij})}{qR_{ij}}, \tag{3}$$

in which q and R_{ij} are the moduli of $\boldsymbol{q}$ and $\boldsymbol{R}_{ij}$, respectively. The IAM equations can be easily derived from the first Born (B1) approximation in scattering theory. In B1, the scattering amplitude is a real number. Since the phase is essential for the interference and accurate elastic scattering amplitudes from an atomic target are easily obtained, "exact" atomic scattering amplitudes will be used.

Note that the molecular interference term does not vanish after the angular average over Ω_L. This was pointed out early by Cohen and Fano in 1966 [29]. From Eq (3), we note that the electron-diffraction image obtained from randomly distributed molecules depends only on the magnitude of the interatomic separations. By taking the inverse sine transform

of the scattering image, the radial distribution function of the molecule can be obtained [3,26,28]. This is the essential idea behind GED theory.

In GED, there are a few well-known limitations. Since the experimental data can cover only a range of angles, or more precisely, a limited range of q, each peak in the retrieved radial distribution function acquires a width. Thus if several interatomic separations are nearly identical, they cannot be separated. Second, the diffraction image is obtained from the contributions of all the atoms. For light atoms, they do not deflect high-energy incident electrons significantly. Therefore, the position of light atoms is more difficult to determine in GED. This is also true for x-ray diffraction.

Since the molecular structure parameters (meaning bond lengths, bond angles, and/or torsion angles) are determined from the molecular interference term, we can define a molecular contrast factor (MCF),

$$\gamma = \frac{1}{I_A} \sum_{i \neq j} f_i f_j^* \frac{\sin(q R_{ij})}{q R_{ij}}. \tag{4}$$

The value and the number of oscillations in MCF will determine the quality of the retrieved molecular structure parameters. Clearly the oscillations are determined by the parameters qR_{ij}. In typical GED, q takes the range of 1 to 30 Å^{-1} [26], but others take as small as 2.2 to about 10 Å^{-1} [12]. For small q, the IAM is not expected to work since the effect of chemical bonding will come into play. For large q, especially for higher energies, the scattering is too weak. This points out that there is no need to use electrons with energies as high as hundreds of keVs as in GED in principle. One can obtain the same range of q using lower electron energies, but for large scattering angles. For typical GED, there is no obstacle to going to higher energies. In fact, a high-energy electron is easier to manipulate and it has a smaller de Broglie wavelength. However, to make short pulses out of high-energy electron beams would be much more of a challenge.

As indicated in the Introduction, our goal here is to obtain diffraction images using the returning electrons generated by a laser pulse. To get a large q for low-energy incident electrons, the scattering angle θ should be large. These are exactly the processes of how HATI electrons are generated.

In Fig. 1(a), we depict the relation between the classical impact parameter and the scattering angle for different incident electron energies, using a neutral carbon atom target as an example. We define that an electron can "see" the carbon atom center when the impact parameter is less than 0.5 a.u. The upper shaded area defines the angular range for incident electron energies from 100 to 300 eV where the IAM can describe the DCS adequately. To the right of the vertical line, the effect of chemical bonding and the many-electron correlation effect are expected to play important roles in electron scattering; thus the simple IAM does not work. In actual measurements, the magnitude of the DCS is also important. In Fig. 1(b) the DCS is plotted against the momentum transfer q. Note that, to first order, the DCS depends on q only, not on electron energies. If we set the lower limit to be the horizontal line shown in the figure, above that the DCS can be

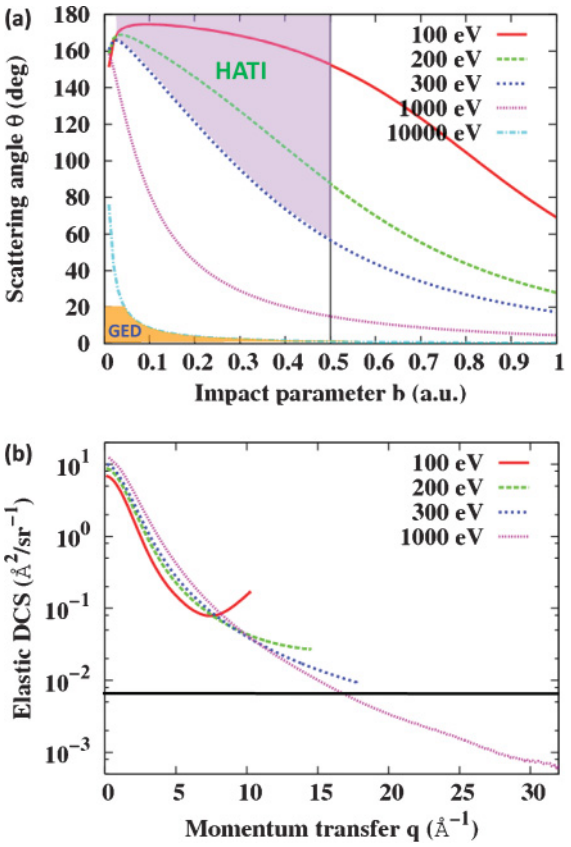

FIG. 1. (Color online) (a) Relation between classical impact parameter b and scattering angle θ for an electron scattered by the potential of a carbon atom. Different curves for incident energies from 100 eV to 10 keV are shown. The vertical line is used to "define" close collisions. The region in scattering angles where GED and HATI spectra can be used for electron-diffraction studies are indicated. (b) Differential cross sections against momentum transfer q for a carbon atom at different incident energies. For small q, the DCS depend on q only. For large q, the DCS depend on q and on incident energy. The horizontal line is drawn to indicate the limit where the DCS can be conveniently measured.

measured, or to q at about 16 Å^{-1}, then the DCS for higher q will be too small. For example, for 10 keV electrons, 20° is about the largest angle where DCS can be used for structure retrieval.

If we take the maximum q at 16 Å^{-1} in Fig. 1(b) to be the lower limit where a diffraction image can be taken, then we can define the region in Fig. 1(a) where the IAM will work for collision energies between 100 and 300 eV and the region for GED when the energy is above 10 keV. In GED it occupies the lower left portion of this allowed region, while for HATI it is in the upper right corner region. Diffraction images taken outside of this shaded region are not useful: either the signal is too weak, or the many-electron correlation as well as the chemical bonding will affect the images, and they would be too difficult for structure retrieval. In Sec. III A the validity of the IAM will be examined for collision energies near 100 eV. If the IAM works, then the same method used in GED can be used for diffraction images taken at the lower incident energies.

B. Quantitative rescattering theory for extracting laser-induced electron-diffraction images

The basic idea of using infrared lasers for imaging the structure of a molecule is based on the rescattering model, or the three-step model [16,17]. When a molecule is exposed to an infrared laser pulse, electrons that were removed at an earlier time may be driven back by the oscillating electric field of the laser to recollide with the parent ion, to incur various electron–ion-scattering phenomena. The simplest one is the elastic scattering of the returning electrons by the target ion. If these electrons are scattered at large angles, that is, if the electrons are backscattered, they will emerge as HATI electrons. These HATI electrons have been studied since the 1990s [30]. Using the quantitative rescattering (QRS) theory recently developed [14,24], we have been able to demonstrate that the photoelectron angular distributions $D(k,\theta)$ can be expressed as

$$D(k,\theta) = W(k_r)\sigma(k_r,\theta_r). \tag{5}$$

Since its first introduction [23], this factorization has been derived by others under different approximations [31–34]. For simplicity, Eq (5) has been written for atomic targets and for a linearly polarized laser. It is understood as describing a beam of incident electrons with momentum distribution given by $W(k_r)$, which is scattered by the ion and emerges with photoelectrons of momentum k and angle θ, and $\sigma(k_r,\theta_r)$ is the field-free differential-scattering cross section. Since scattering occurs in the laser field, the scattered electron gains an additional momentum from the laser field. This additional momentum is given by $-A(t_r) = -A_r$, where t_r is the instant of electron recollision. Thus the relation between the momentum of the photoelectron and the momentum of the scattered electron right after the collision is given by

$$\begin{aligned} k_z &= k\cos\theta = -A_r \pm k_r\cos\theta_r, \\ k_y &= k\sin\theta = k_r\sin\theta_r, \end{aligned} \tag{6}$$

where the plus (minus) in the upper equation accounts for electrons returning to the target along $+\hat{z}$ $(-\hat{z})$. Here the z axis is defined to be along the laser polarization axis. According to QRS, $k_r = 1.26A_r$. Based on the Eqs. (5) and (6), one can obtain field-free elastic-scattering differential cross sections $\sigma(k_r,\theta_r)$ for a given k_r from the momentum distributions $D(k,\theta)$ of the photoelectrons.

The validity of the QRS model has been carefully tested [14,24]. Since $\sigma(k_r,\theta_r)$ is the same as one would obtain from the collision of a beam of free electrons with the target ion, the QRS model establishes that one can obtain electron-diffraction images from the momentum spectra of HATI electrons [35–37]. Most importantly, according to the QRS model, the extracted diffraction images should be independent of the laser pulses used so long as the spectra are retrieved from the 5–10 U_p region. For a fixed-in-space molecule in a linearly polarized laser pulse, the HATI spectra depend on the polar angle as well as the azimuthal angle. Since gas-phase molecules are either isotropically distributed or only partially aligned or oriented, the HATI spectra obtained should include such averages. In Eq. (5), the magnitude of the wave packet depends on the tunneling ionization rate, which in turn depends on the orientation or alignment of the molecules. Thus the electron-diffraction images extracted from HATI spectra should be weighted by tunneling ionization rates. For isotropically distributed molecules this is

$$\begin{aligned} \langle I_{\rm tot}\rangle(\theta) = &\left(\sum_i |f_i|^2\right)\int N(\Omega_L)\,d\Omega_L \\ &+ \sum_{i\neq j} f_i f_j^* \int e^{i\boldsymbol{q}\cdot\boldsymbol{R}_{ij}} N(\Omega_L)\,d\Omega_L, \end{aligned} \tag{7}$$

where $N(\Omega_L)$ are the tunneling ionization rates calculated using the molecular Ammosov-Delone-Kralnov (MO-ADK) theory [38,39], and Ω_L are the orientation or alignment angles with respect to the polarization direction of the laser beam, the same as in Eq. (1). A corresponding molecular contrast factor can also be defined using

$$\gamma = \frac{\sum_{i\neq j} f_i f_j^* \int e^{i\boldsymbol{q}\cdot\boldsymbol{R}_{ij}} N(\Omega_L)\,d\Omega_L}{\left(\sum_i |f_i|^2\right)\int N(\Omega_L)\,d\Omega_L}. \tag{8}$$

If the molecules are partially oriented or aligned, clearly the angular distribution should be included in the integral over Ω_L.

C. Structure retrieval using genetic algorithm

In Sec. III, with the diffraction images from electron collisions with molecules, or from the HATI spectra, we also conducted several retrieval tests using the genetic algorithm (GA). The GA driver, GA v1.7a, was implemented by Carroll [40] with FORTRAN language, which has both Simple GA and micro-GA options. We actually used micro-GA [41], which evolves small populations (typically four to ten individuals).

In our approach, a Z matrix is chosen to build up the geometry of an isolated candidate molecule, which consists of bond lengths, bond angles, and torsion angles. These structural variables, named by $\boldsymbol{X}$, form a search space (parametric space). In general, a molecule, especially an N-atom nonlinear molecule has $3N-6$ degrees of freedom. The fitness function $\chi^2(\boldsymbol{X})$ is defined by the least squares of the difference between the experimental data and the calculated DCS with a trial structural parameter set, but since the experimental DCS doesn't have absolute values, a scaling factor is needed to bring it onto the same scale as theoretical DCS [41]. The fittest candidate geometry is the one which gives the lowest χ^2 value (meaning best agreement with an experimental diffraction image).

The micro-GA starts an evolution with an initial population, which is randomly picked up from the parametric space, and the fitness value of each individual then is calculated, giving an evaluation of the quality of each trial structure. In the next step, parents are selected according to their fitness values, and micro-GA always bias the fitter candidates, which is the so-called "survival of the fittest." A uniform crossover operator is then applied to each pair of two mates to produce new generations. The crossover procedure is performed on the basis of binary encodings instead of on the basis of real-valued encodings, and each bit in the binary representation of each parametric set represents a gene. Elitism is also applied to retain the current fittest structure in the next generation, which is expected to efficiently wipe out the negative effect of crossover. Once a new generation is created, the micro-GA

starts another evolution loop with it as the parent generation. This goes on up to some preset number of generations. It ends with the output of the best geometry. Since the micro-GA evolves with a small population, premature convergence can happen easily; that is, different individuals converge to an identical local minimum. To prevent this, the micro-GA will check the similarity of the whole population for each generation, by comparing the genes of the current best fit with the other individuals locus by locus. If the number of nonidentical bits is less than 5% of the total bit number, the micro-GA will restart with the best fit and randomize the rest. More details may be found in [41]. This method has been used to reconstruct atoms [41,42] from the atomic DCS at large angles.

III. RESULTS AND DISCUSSION

A. Electron-molecule scattering and IAM model for isotropically distributed molecules

1. CO_2

We first check how well the IAM works for electron collisions with neutral molecules. Consider electron collisions with CO_2 targets for incident energies of 20, 50, 100, and 200 eV. In Fig. 2 are shown the IAM results compared with the experimental data taken from Register *et al.* [43], Iga *et al.* [44], Kanik *et al.* [45], and Tanaka *et al.* [46]. Only data for large angles are shown. In the IAM calculations, the interaction potential between the incident electron with the carbon atom is approximated by a Yukawa potential with the parameter λ listed in Table I. The λ for other atoms used in this article are also given in this Table. It is chosen such that the ground-state energy of the negative ion calculated has the best agreement with the experimental data [47]. The calculation of the scattering amplitude for each atom can be found in standard quantum mechanics textbook, for example, [48], or in Sec. II D of [24]. In the IAM simulation, the bond lengths are taken from the experimental data. From Fig. 2, it is clear that the IAM does not give a good description of the DCS for collisions below 50 eV. At 100 eV and higher, the agreement becomes quite good. In the covered energy region, the DCS becomes larger at large angles, with a pronounced broad minimum. This broad minimum is due to the diffraction from individual atoms. This is different from collisions at the hundreds of keVs used in GED where the DCS decreases monotonically at large angles.

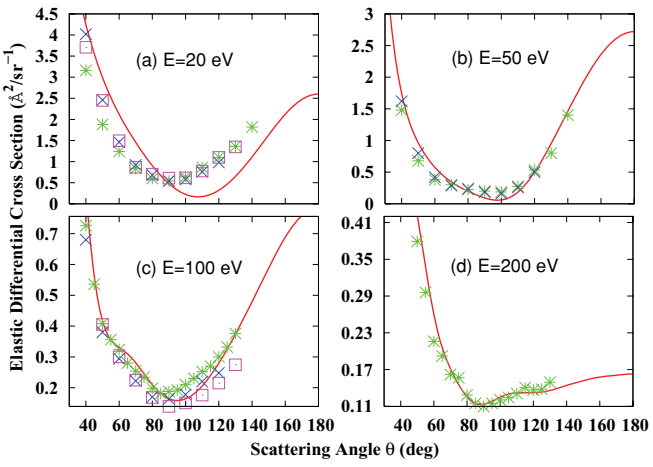

FIG. 2. (Color online) Elastic differential cross sections for e^--CO_2 collisions at incident energies of 20, 50, 100, and 200 eV. Solid red curves are IAM simulation. Symbols are experimental data from different groups. Asterisks: (a,b) from Register *et al.* [43], (c,d) from Iga *et al.* [44]; crosses: from Kanik *et al.* [45]; empty squares: from Tanaka *et al.* [46].

TABLE I. Parameters in Yukawa potential $V(r) = -Ze^{\lambda r}/r$ for selected atoms. The nuclear charge Z and a damping factor λ are listed.

	Z	λ (a.u.)
H	1	0.881
Li	3	0.774
C	6	1.276
N	7	1.695
O	8	1.720
F	9	1.902

In Fig. 2, there is no clear evidence of molecular interference in the experimental DCS. In Figs. 3(a) and 3(b) we display the same experimental DCS from Iga *et al.* [44] and compare them to the atomic term, for collision energies of 100 and 200 eV. One can see that the IAM predictions and the experimental data oscillate about the atomic DCS. Recall that these results are for isotropically distributed CO_2. It demonstrates that molecular interference survives the average over the randomly distributed molecules.

To appreciate the difference of the DCS calculated from the simple IAM with the experimental data, we subtract the atomic DCS and show the difference as the molecular interference term. For this purpose, we renormalize the experimental data by a multiplicative factor α,

$$I_{\mathrm{MIT}} = \alpha I_{\mathrm{tot}}^{\mathrm{exp}} - I_{\mathrm{tot}}^{\mathrm{atom}}. \tag{9}$$

Factor α is chosen such that the mean square of the difference between the renormalized experimental data and the atomic DCS is at a minimum. The resulting molecular interference term from the experimental data and from the IAM are shown in Figs. 3(c) and 3(d). Note that both the IAM and the experimental data show oscillations. There are shifts in the oscillations between the data and the IAM predictions which we take to indicate the inaccuracy of the IAM at these energies. At 200 eV we can see the difference is smaller. This result is expected since the IAM is a model built upon the high-energy scattering theory.

We can also display the molecular contrast factor, MCF, see Eq. (4), for the experimental data and the IAM prediction, shown in Figs. 3(e) and 3(f). It shows that there is a shift in the oscillations between the data and the IAM, more so at 100 eV than at 200 eV. Presenting MCF allows us to evaluate the degree of fluctuations in the experimental data. Clearly the last experimental point in Figs. 3(f) is too high. In practical GED applications, experimental data are often first smoothed [28] before they are used to retrieve the radial distributions of molecules.

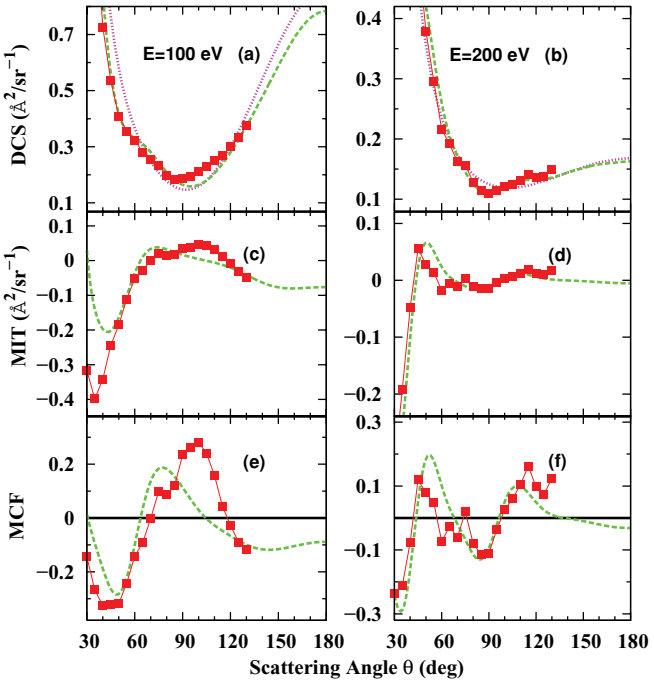

FIG. 3. (Color online) (a,b) Experimental (red solid squares) and theoretical (dashed green curves) DCS vs the atomic terms (dotted pink curves). (c,d) Molecular interference terms, comparing experimental data with the IAM. (e,f) Same as (c) and (d) but for molecular contrast factors.

2. C_2F_6

We next consider a more complex molecule like C_2F_6 where elastic differential cross sections for e^--C_2F_6 collisions have been reported by Iga *et al.* [49]. In Fig. 4(a) the shape of this molecule is depicted, and values of the molecular interference terms from the experiment and from the IAM are shown at three collision energies of 150, 200, and 300 eV in Figs. 4(b)–4(d). It is interesting to note that for the angular range of 30° to 70° there is a pronounced interference maximum and minimum, respectively, at each energy. At larger angles the molecular interference term is quite flat. At these energies there is a general agreement between the IAM prediction and experiment.

The similarity of the molecular interference term in Figs. 4(b)–4(d) is not surprising. In Fig. 4(e) we plot the DCS obtained from the IAM in terms of the momentum transfer q for the three energies. One can see that within a range of q, they lie on top of each other. Only at large angles do we see deviation from the universal curve. We comment that, within the first Born approximation, the DCS depends only on q, not on the scattering energies and angles independently. In Fig. 4(f) we plot the experimental data against q. It shows that they lie on a universal curve mostly, very similar to the predictions of the IAM.

More tests on the validity of the IAM over the intermediate-energy region were carried out elsewhere, for example, in [50–52]. Especially in [52], Iga *et al.* presented an experimental verification on the applicability of the IAM in the previously mentioned energy region, with DCS for acetylene, *n*-butane, and benzene being measured.

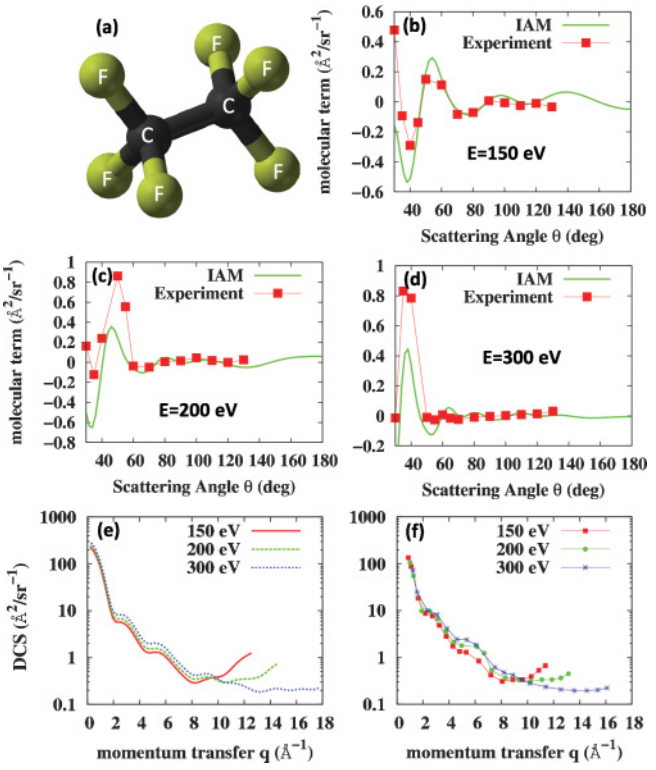

FIG. 4. (Color online) (a) Structure of a hexafluoroethane C_2F_6 molecule in a ball-and-stick model. (b, c, d) Molecular interference terms for e^--C_2F_6 collisions, experimental data [49] vs IAM, at incident energies of 150, 200, and 300 eV. Elastic DCS plotted against momentum transfer q, IAM (e) vs experimental data (f), for the three energies, respectively.

3. *Retrieval of bond length from the DCS of randomly distributed molecules*

In this subsection, we address how much error is introduced on the retrieved interatomic separations if we assume that the experimental DCS is described by the IAM. Note that we use the GA for the retrieval instead of the inverse sine transform used in GED. Here we first take the simple example of CO_2. Using the experimental DCS the retrieved C–O bond length is 1.28, 1.08, and 1.13 Å, using experimental data at 50, 100, and 200 eV, respectively (see Table II). Compared to the known bond length of 1.163 Å, the errors are +10%, −6.7%, and −2.9%, respectively. Such accuracy is inferior to what can be accomplished using GED. Note that there are very few experimental data points used in the retrieval and data at many larger angles are not available. These experimental data were not taken for the purpose of GED; thus there are few data points at large angles. Despite this, a reasonable C–O bond

TABLE II. Retrieved C–O bond length of CO_2 from experimental DCS at 50, 100, and 200 eV, respectively.

	C–O bond length (Å)
Experiment	1.163
50 eV	1.28(+10%)
100 eV	1.08(−6.7%)
200 eV	1.13(−2.9%)

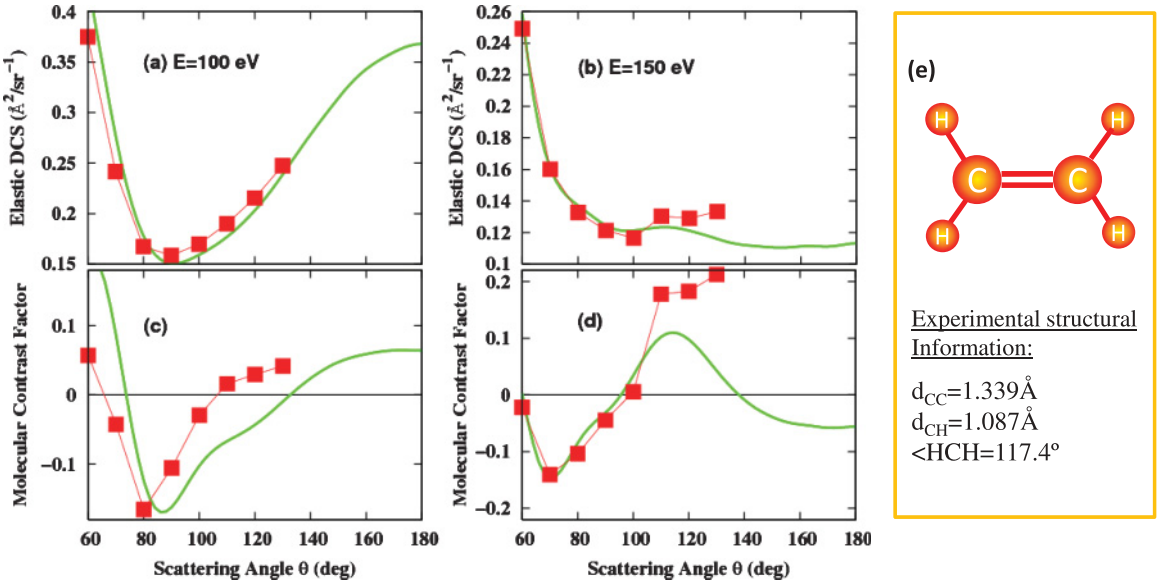

FIG. 5. (Color online) (a,b) Comparison between measured DCS (red solid squares) of C_2H_4 at electron incident energies of 100 and 150 eV and the IAM simulations (green solid lines). (c,d) Comparison of the molecular contrast factors. The known bond lengths and the bond angle are shown in (e).

length can already be retrieved. For future dynamic imaging, such errors are acceptable since the goal there is to follow the change of bond length with time, rather than the precise values at a given time.

For another example, we considered ethylene. In Fig. 5(e) the known structure of C_2H_4, the C–C and C–H bond lengths, and the angle HCH are given. This system is considered to be a challenge for GED since the DCS from H is much smaller than that from C, such that information on H is difficult to retrieve. In Figs. 5(a) and 5(b) we show the DCS data from e^--C_2H_4 collisions for incident energies at 100 and 150 eV from Brescansin *et al.* [53], as well as the prediction of the IAM using the known molecular parameters. The same results are shown in terms of the molecular contrast factors γ in Figs. 5(c) and 5(d). Using the experimental DCS from Figs. 5(a) and 5(b) and the GA, we retrieve the molecular parameters and the results are shown in Table III. At 100 eV, the retrieved data have 7% error in the C–C bond length, while the C–H length and the angle HCH have larger errors. However, the retrieved results using the experimental data at 150 eV look very good. Here we use the DCS directly for the fitting. If we use the molecular contrast factors in Figs. 5(c) and 5(d) for the fitting, we obtained the different results as shown in the bottom two rows in Table III. The discrepancies between the two methods are not surprising. The fitness functions in the two approaches are not the same. By fitting the DCS, the fitness function emphasizes small angles where the DCS are larger. Using the MCF, all the angles are treated on equal footing. Thus the error at large angles in Fig. 5(c) is enhanced in the retrieval.

TABLE III. Retrieved structural information of C_2H_4 from experimental DCSs at 100 and 150 eV, respectively, compared to the known experimental values. The first set is obtained from fitting the molecular interference term; the second set is from fitting the molecular contrast factor (see text).

	C–C length (Å)	C–H length (Å)	∠ HCH
Experiment	1.339	1.087	117.4°
100 eV	1.436(7%)	1.281(18%)	144.4°
150 eV	1.324(−1%)	1.075(−1%)	105.8°
100 eV	1.058(−21%)	0.947(−13%)	163.7°
150 eV	1.271(−5%)	1.134(4.3%)	109.0°

As mentioned earlier, we used the GA to retrieve the molecular structure parameters from the electron-diffraction images. It turns out that the GA has been suggested recently for molecular structure retrieval for diffraction images taken using GED or UED [54,55]. The global GA search for molecular geometries of a dynamic system is especially powerful since data retrieved from an earlier time step can be used to impose constraints on the search space in the next step to achieve faster convergence. By using techniques developed from the larger GED and UED communities, the retrieval of molecular structure from the HATI spectra will be able to proceed significantly faster when experimental data become available.

4. Dependence of DCS on bond lengths or angles in the molecule

It is interesting to note that electron-diffraction images are very sensitive to the interatomic distances for a given molecule, as can be seen in Eq. (2) since R_{ij} appears in the phase factor in the IAM. When the positions of the atoms in a molecule change as in a dynamic system, the atomic DCS will remain the same, but the molecular interference term will evolve in time. In Fig. 6(a) we show how the molecular contrast factor changes when the bond distance between C and O is changed in CO_2. Shown are data for electron collisions at 100 eV and for the C–O length that has been increased or decreased from its normal value by 10% and 20%, respectively. As the bond length increases, the oscillation shifts to smaller angles and the oscillation becomes faster. This is easily understood from

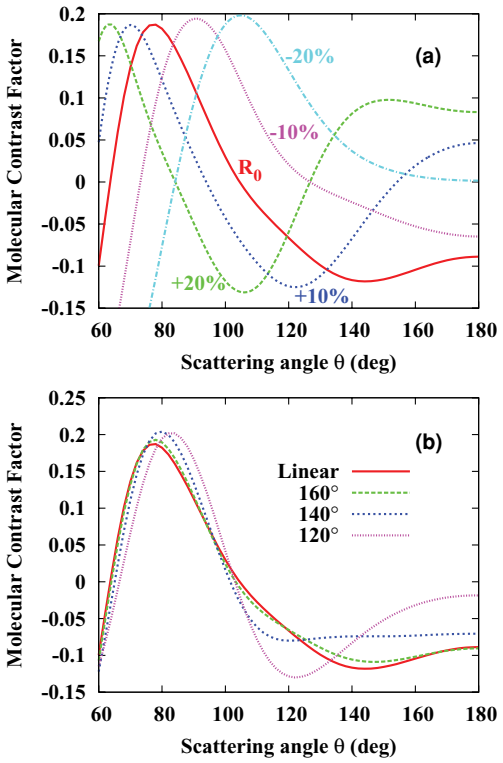

FIG. 6. (Color online) (a) Sensitivity of the molecular contrast factor γ vs the change of C–O bond length for e^--CO_2 collisions at 100 eV. The bond length has been increased or decreased by 10% and 20% with respect to the equilibrium value, respectively. (b) The same, but for a triangular CO_2, where the bond angle OCO is varied.

the IAM since the phase $\boldsymbol{q} \cdot \boldsymbol{R}_{ij}$ in Eq. (2) increases with the bond length.

We have also examined the case where the CO_2 is assumed to be nonlinear [see Fig. 6(b)]. We change the bond angle while the C–O bond length is kept fixed. This is equivalent to decreasing the internuclear distance of O–O. The conclusion is the same. When the change of bond length is large, the molecular contrast factor γ changes more rapidly. For large angles, say from 180° to 160°, the change in O–O distance is small, and thus γ does not change much. For θ from 140° to 120°, the γ changes much more since the O–O bond length changes more.

B. Electron-molecule scattering and IAM model for aligned or oriented molecules

1. Electron-diffraction images from molecules aligned in one dimension

The preceding discussions focused on molecules that are isotropically distributed. If the molecules are oriented or aligned, clearly the diffraction images will have more pronounced interferences. Field-free molecules can be partially aligned or oriented by infrared lasers [25], or by photodissociation [11,12] using linearly polarized lights. For simplicity, here we consider molecules aligned in one dimension only. This can be carried out by exposing molecules to a short linearly polarized infrared laser. After the pulse is over, the molecules will change from aligned to antialigned (or vise versa) near the time intervals of rotational revivals. In 1D alignment, the molecules are distributed cylindrically symmetric with respect to the polarization axis (the z axis) of the aligning laser. We consider electron collisions with these aligned molecules, where the incident electrons are directed along the z axis. In this simple geometry, the DCS depends on the polar angle θ only, not on the azimuthal angle ϕ. We mention that we are not aware of any such measurements yet. For molecules aligned by photodissociation, there have been a few reported so far, with the time resolutions of a few hundred femtoseconds [11,12].

In Fig. 7(a) we show the calculated DCS for electron collisions with aligned CO_2 molecules at incident energy of 100 eV, for molecules aligned parallel and perpendicular to the z axis, respectively. We assume that the angular distribution of the molecules has the $\cos^6(\theta_L - \theta_{L0})$ dependence, where θ_L is the angle between the molecular axis and the incoming direction of the electron beam and θ_{L0} is the central angle of the aligned molecules. In this figure, the DCS for the atomic terms only and the DCS for isotropically distributed molecules are also shown.

From Fig. 7(a), it is interesting to note that the oscillation is much stronger for parallel-aligned molecules than for the perpendicularly aligned molecules. This is expected for all linear molecules and can be understood from the IAM. In Eq. (2), the phase of the interference term is given by $\boldsymbol{q} \cdot \boldsymbol{R}_{ij}$. For large scattering angles, the momentum transfer vector $\boldsymbol{q}$ is nearly antiparallel to the incident direction. Thus $\boldsymbol{q} \cdot \boldsymbol{R}_{ij}$ is near zero if the molecule is perpendicularly aligned and

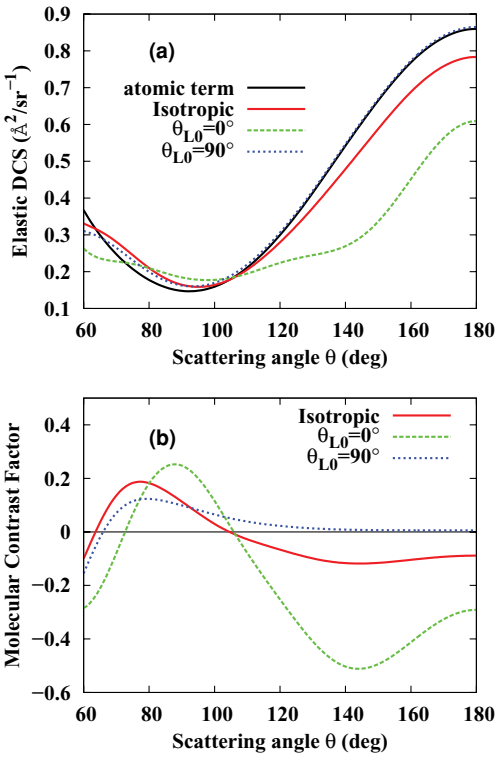

FIG. 7. (Color online) (a) Comparison of DCS for parallel-aligned, perpendicularly aligned, and isotropic CO_2 molecules. The atomic term is also shown (barely separable from the 90° curve at large angles). (b) Same data presented in terms of molecular contrast factor.

maximum when it is aligned. This is opposite to GED where the electron is scattered in the forward directions and $\boldsymbol{q}$ is nearly perpendicular to the incident direction. In this limit, more favorable interference is expected when molecules are perpendicularly aligned. Thus for linear molecules, to obtain large molecular contrast, sharper features in the diffraction images are obtained by aligning molecules parallel to the incident electrons if the electron energy is below 300 eV and the images are taken in the backward directions. For completeness, in Fig. 7(b) we show the MCF obtained from the DCS shown in Fig. 7(a).

For another example, we compare the MCF for aligned C_2F_6, again assuming the molecules have one-dimensional alignment and have angular distributions given by $\cos^6(\theta_L - \theta_{L0})$. We consider the alignment axis (the C–C axis) making an angle 0°, 45°, and 90°, respectively, with the incident electron beam entering along the z axis. The IAM is used to calculate the DCS. From the DCS calculated, we extract the MCF for the three alignment angles and the isotropic one. The resulting molecular contrast factors versus the scattering angles are shown for scattering energies of 100 and 200 eV, in Figs. 8(a) and 8(b), respectively. It is noted that for an alignment angle of 45°, the contrast is about the same as that for the isotropic one. The contrast is still the largest when the molecules are parallel aligned. Unlike the linear molecules, the contrast for the perpendicularly aligned molecules is no longer small. For this molecule, if the molecule is perpendicularly aligned, the C–C axis is perpendicular to $\boldsymbol{q}$, but the C–F bond is parallel to $\boldsymbol{q}$. Comparison of Figs. 8(a) versus 8(b) shows that there are more interference maxima and minima at higher scattering energies.

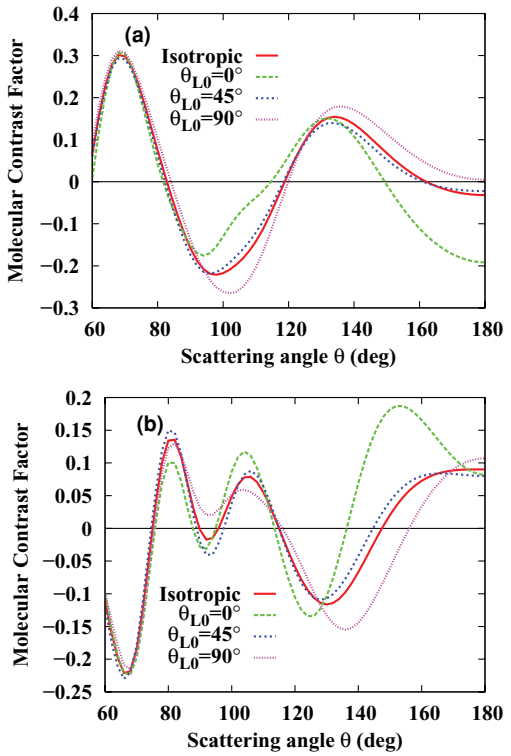

FIG. 8. (Color online) (a) Comparison of MCFs of C_2F_6 molecules under different alignment conditions for an incident energy of 100 eV. (b) Same as in (a) but for 200 eV.

2. *Retrieving molecular bond lengths (and bond angles) from electron-diffraction images of molecules aligned in three dimensions*

So far we have shown that the diffraction images from randomly distributed molecules are very sensitive to the bond lengths of the constituent atoms in the molecule. Clearly the structure retrieval will be significantly improved if diffraction data for aligned or oriented gaseous molecules are available [56].

For simplicity, here we illustrate how the atomic positions in a molecule can be retrieved if the DCS are available from fixed-in-space molecules. In Fig. 9(a) we construct a fictitious isomerization scenario. For the linear LiCN molecule, we assume that it evolves to CNLi along the (arbitrarily chosen) path indicated in the figure. In the simulation, we place Li at a new position and restrict it to move only on the plane of the figure [57]. We use the IAM to obtain the two-dimensional (2D) electron-diffraction image for each new position, assuming that the electron beam is perpendicular to

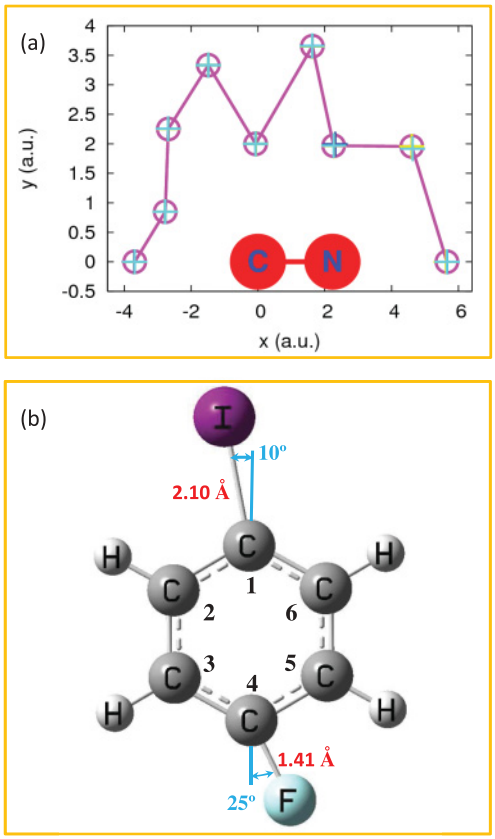

FIG. 9. (Color online) (a) Simulation of the isomerization of LiCN to NCLi. In the model, the plane of the molecule is fixed and the laser's polarization is perpendicular to it. The assumed path taken by Li is given by open circles at different steps. From the HATI spectra, the retrieved Li positions from GA are indicated by crosses. (b) A model of a 1-fluoro-4-iodobenzene molecule away from its equilibrium configuration. We assume that the iodine and fluorine atoms are at the positions indicated. Laser polarization is perpendicular to the plane. From the "measured" HATI spectra, this molecular geometry is reconstructed, with results shown in Table IV.

TABLE IV. From the "measured" HATI spectra of 1-fluoro-4-iodobenzene, the retrieved parameters usin the GA are compared to the input parameters.

	Ordering	(d_{CI},θ_I)	(d_{CF},θ_F)
"Real"	IHHFHH	(2.10 Å, 10.00°)	(1.41 Å, 25.00°)
Retrieved	IHHFHH	(2.10 Å, 9.94°)	(1.41 Å, 24.96°)

the plane. We then introduce a 10% random error to each image data point and treat the results as experimental data. We use the GA and the IAM to retrieve the position of Li, that is, the distance of Li-C and the angle LiCN, with the C–N bond fixed. In Fig. 9(a), the input position of Li is denoted by the center of each circle; the retrieved position is indicated by the crosses. For this example, retrieval of the position of Li is quite simple.

In another example, we consider a planar 1-fluoro-4-iodobenzene molecule, C_6H_4IF [see Fig. 9(b)], away from its equilibrium configuration. This is a benzene molecule where one of the H atoms is replaced by fluorine and another replaced by iodine. We will assume that the C–C bond and the C–H bond do not change, but allow the I and F to change from their normal equilibrium positions as indicated. In the hypothetical experiment, we assume that the incident electrons enter perpendicularly to the plane of the molecule. We use IAM to calculate the DCS (2D spectra), and we introduce 10% random errors to each image point and take the results as "experimental" data. In the retrieval, we allow F to switch to a different C site. Here we define the position of the C that is connected to I to be No.1, as indicated in the figure. Using the GA, in this example, the search involves five parameters: the two angles and the two bond lengths indicated in the figure for I and F, respectively, and the order of the C atom where the fluorine is attached. From Table IV we note that the five input parameters are accurately retrieved.

The simulation in Fig. 9(b) represents a large class of chemical compounds where the hydrogen atoms are replaced by heavy atoms. Since diffraction images from individual heavy atoms are much larger [see Fig. 10(d)], the difference image shown in Fig. 10(a) is quite large when the positions of heavy atoms are changed. In Fig. 10(b) the diffraction image taken when F and I are away from their equilibrium positions is compared to Fig. 10(c), where F and I are in their normal positions. The simulations were carried out at an incident electron energy of 200 eV, and the beam is perpendicular to the plane of the molecule. At 200 eV, the DCS for C and F are monotonically decreasing with increasing angles, but not for the heavy iodine atom [see Fig. 10(d)]. In the present simulation, a two-term Yukawa potential was used to represent the iodine atom potential.

We have assumed that the molecules are fixed in space. But it is straightforward to generalize the analysis to partially aligned or oriented molecules, as well as other directions for the incident electron beams. In the next subsection, we show that such flexibility can be easily carried out if the electron beams are replaced by laser-induced rescattering electrons.

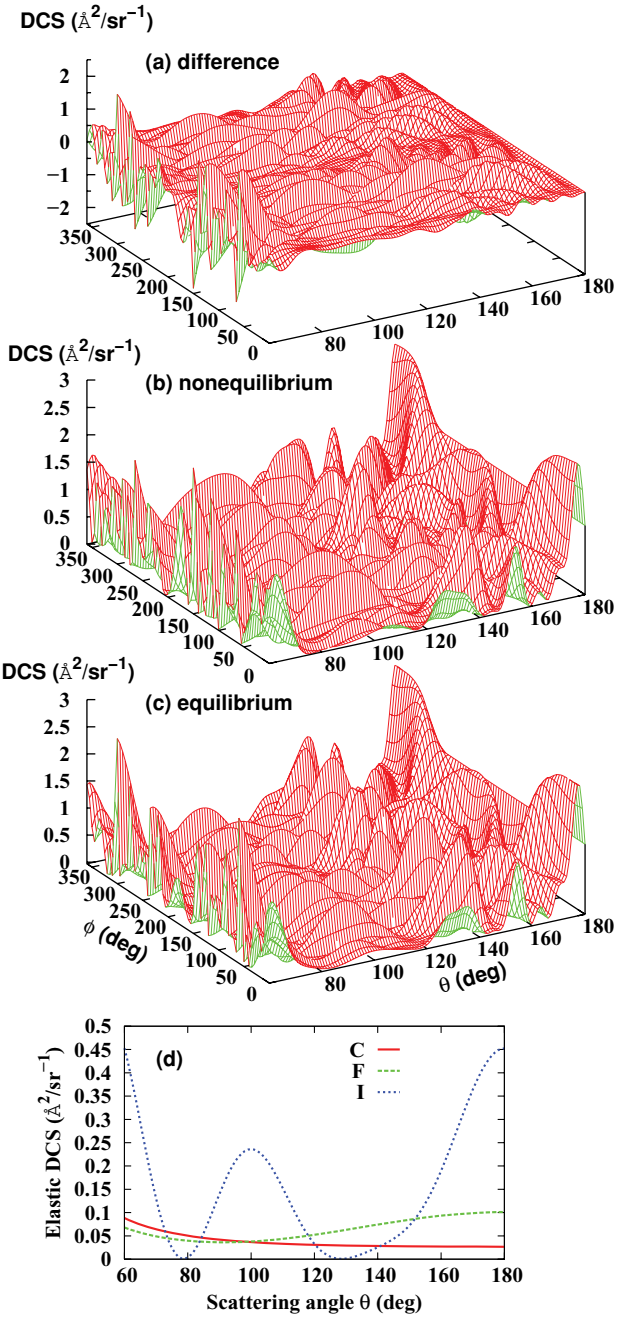

FIG. 10. (Color online) (a) The difference of the DCS for electrons colliding with 1-fluoro-4-iodobenzene with I and F atoms at and away from their equilibrium positions. (b,c) The diffraction spectra for F and I at the nonequilibrium (b) and the equilibrium (c) configurations. (d) Comparison of the differential cross sections for iodine, fluorine, and carbon atoms. The electron energy is 200 eV.

C. Electron diffraction using rescattering electrons generated by molecules in an intense laser field

As explained in Sec. II B, one can extract field-free DCS, or the diffraction image, of a molecular ion, say CO_2^+, from the HATI electron momentum spectra, by exposing CO_2 molecules to a linearly polarized laser pulse. Within the short time (about three quarters of an optical cycle, that is, within about 1 fs) it takes the rescattering electron to return to

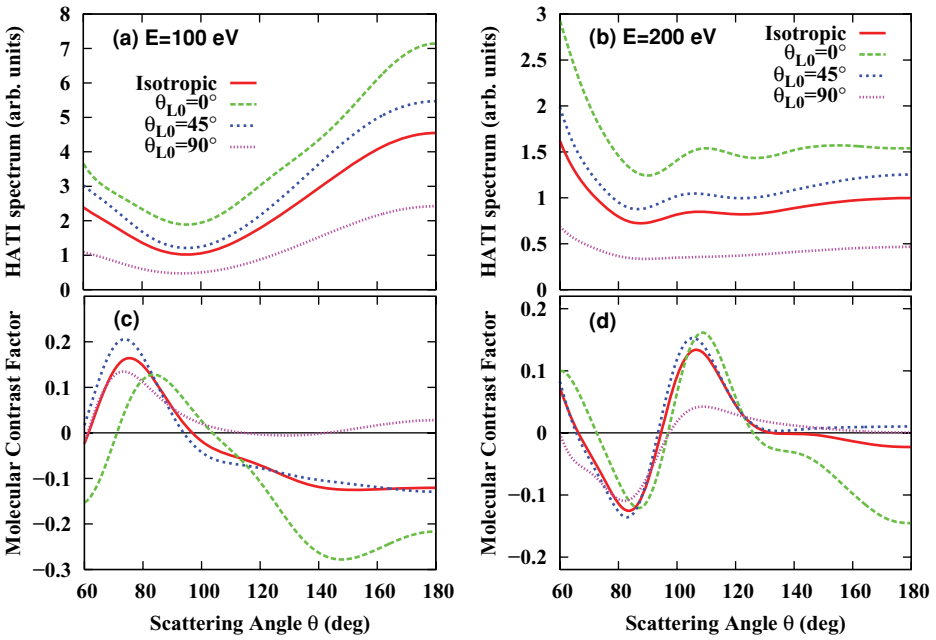

FIG. 11. (Color online) (a,c) Simulation of HATI spectrum of CO_2 at returning electron energy 100 eV and its corresponding MCF, based on QRS theory with ionization rate included, which is calculated using MO-ADK theory. (b,d) Same as (a) and (b) but at returning energy of 200 eV.

recollide with the ion, we can safely assume that the atomic positions in the molecule do not change. Thus the diffraction images taken for the ion would reflect the atomic positions of the molecule directly.

In Fig. 11 we consider partially aligned CO_2 molecules with a distribution assuming to be given by $\cos^6(\theta_L - \theta_{L0})$ as before. From the HATI spectra we can extract the diffraction images, or the DCS. The results for returning energies of 100 and 200 eV are shown for a number of alignment angles and for isotropic molecules [see Figs. 11(a) and 10(b)]. The corresponding MCFs are also shown [see Figs. 11(c) and 10(d)]. The alignment-dependent tunneling ionization rates used in obtaining Fig. 11 are taken from [39].

To simulate the HATI spectrum, we need to calculate elastic-scattering cross sections for $e^- + CO_2^+$ collisions. Unlike the CO_2 target, when the incident electron is far away from CO_2^+, it sees a $-1/r$ potential. Thus it is generally expected that the DCS for $e^- + CO_2^+$ and $e^- + CO_2$ are quite different. This is true for DCS at small angles where the incident electron probes the outer-shell region. For HATI spectra, the returning electrons are backscattered. They are scattered near the atomic core where the potential is much larger than the $-1/r$ potential. Thus we expect the difference in the DCS between neutral and singly charged ions to be negligible for these deep-penetrating scattered electrons. We have checked this conclusion for atomic targets, for energies near and above 100 eV. For our purpose here we check CO_2 in a different way. In Fig. 11, we calculated the DCS for $e^- + CO_2^+$ collisions, using the IAM model for O–C^+–O, O^+–C–O and O–C–O^+, and the results are averaged. The bond length between C–O was set at 1.163 Å. We treat such results as experimental data and use the IAM model for neutral CO_2 to retrieve the bond length of C–O, using angle-averaged DCS and the GA. The retrieved bond length was 1.149 Å. In other words, unless we are searching for much higher precision, we may as well just use the IAM for neutral molecules for the retrieval of the structure parameters. We comment that the error for using IAM is expected to become larger if the scattering energy becomes smaller. For atomic ion, for example, C^+, the potential was written as $V(r) = -(1 + 5e^{-1.532r})/r$ where the exponential parameter was obtained by fitting to the ground-state energy of C.

We comment that experimental data from CO_2 for returning electrons with energies at or above 100 eV are not available yet. HATI spectra for CO_2 have been reported by Cornaggia [58] using 800-nm Ti-sapphire lasers. The returning electron energies from this experiment are about 15–30 eV. At such energies the IAM does not work so the C–O bond length cannot be simply retrieved. Other HATI spectra have been reported for randomly distributed [59,60] and for aligned N_2 and O_2 molecules [61], but only for 800-nm Ti-sapphire lasers. Again, these data cannot be analyzed using the model presented here. To reach returning energies of 100 eV or more, midinfrared (MIR) lasers will be needed. Since aligned CO_2 has been used in high-order harmonic generation by MIR lasers already [62,63], it is highly desirable to measure HATI spectra from aligned CO_2 (or any other simple molecules) to test the theory presented here.

IV. SUMMARY AND PERSPECTIVE

In this article we demonstrated that it is possible to use intense infrared and midinfrared lasers to probe the structure of a molecule. The idea is to use the rescattering electrons generated by the laser. Two basic theoretical ingredients are used here. First, based on the quantitative rescattering theory for strong-field physics, it has been shown that the angular distributions of the high-energy photoelectrons generated by the strong field can be used to extract field-free elastic differential cross sections by the rescattering electrons. These are electrons that have been backscattered from the molecular ion. Thus, they are sensitive to the positions of atoms in a molecule, similar to electron-diffraction images generated by a few-hundred-keV electrons in the conventional electron-diffraction method. Second, we have established theoretically

that the simple independent atom model used in GED can be extended to incident energies in the order of 100 eV, so long as we restrict ourselves to electron images taken at large angles. We established the validity of the IAM using electron-scattering data taken in the 100–200 eV region for a few molecules. From these limited data we confirm that they can be used to retrieve the bond length of the molecules. Since infrared and midinfrared laser pulses of durations of a few femtoseconds are already available, this would suggest that IR and MIR laser pulses should be investigated further for their potential for dynamic imaging of transient molecules. Experimentally, current technologies are capable of generating such spectra, for randomly distributed molecules and for aligned molecules. Using CO_2 as an example, we have made the theoretical analysis of HATI spectra from aligned CO_2 molecules. It is desirable that such data become available soon experimentally. This will be the first step toward using MIR lasers for dynamic imaging of molecules.

ACKNOWLEDGMENTS

This work was supported in part by the Chemical Sciences, Geosciences, and Biosciences Division, Office of Basic Energy Sciences, Office of Science, US Department of Energy.

[1] J. Miao, C. Charalambous, H. Kirz, and D. Sayre, Nature (London) **400**, 342 (1999).
[2] J. R. Fienup, Appl. Opt. **21**, 2758 (1982).
[3] *Stereochemical Applications of Gas-Phase Electron Diffraction*, edited by I. Hargittai and M. Hargittai (VCH, New York, 1988), and references therein.
[4] A. H. Zewail and J. M. Thomas, *4D Electron Microscopy: Imaging in Space and Time* (Imperial College Press, London, 2009).
[5] D. Strasser, F. Goulay, and S. R. Leone, J. Chem. Phys. **127**, 184305 (2007).
[6] C. Z. Bisgaard, O. J. Clarkin, G. Wu, A. M. D. Lee, O. Geßner, C. C. Hayden, and A. Stolow, Science **323**, 1464 (2009).
[7] H. Xu, T. Okino, and K. Yamanouchi, J. Chem. Phys. **131**, 151102 (2009).
[8] A. Hishikawa, A. Matsuda, M. Fushitani, and E. J. Takahashi, Phys. Rev. Lett. **99**, 258302 (2007).
[9] M. Fushitani, Annu. Rep. Prog. Chem. Sect. C **104**, 272 (2008).
[10] R. Neutze, R. Wouts, D. van der Spoel, E. Weckert, and J. Hajdu, Nature (London) **406**, 752 (2000).
[11] H. Ihee, V. A. Lobastov, U. M. Gomez, B. M. Goodson, R. Srinivasan, C. Y. Ruan, and A. H. Zewail, Science **291**, 458 (2001).
[12] P. Reckenthaeler, M. Centurion, W. Fuß, S. A. Trushin, F. Krausz, and E. E. Fill, Phys. Rev. Lett. **102**, 213001 (2009).
[13] B. J. Siwick, J. R. Dwyer, R. E. Jordan, and D. Miller, Science **302**, 1382 (2003).
[14] C. D. Lin, A.-T. Le, Z. Chen, T. Morishita, and R. R. Lucchese, J. Phys. B **43**, 122001 (2010).
[15] T. Morishita, A.-T. Le, Z. Chen, and C. D. Lin, New J. Phys. **10**, 025011 (2008).
[16] P. B. Corkum, Phys. Rev. Lett. **71**, 1994 (1993).
[17] J. L. Krause, K. J. Schafer, and K. C. Kulander, Phys. Rev. Lett. **68**, 3535 (1992).
[18] T. Zuo, A. D. Bandrauk, and P. B. Corkum, Chem. Phys. Lett. **259**, 313 (1996).
[19] S. X. Hu and L. A. Collins, Phys. Rev. Lett. **94**, 073004 (2005).
[20] M. Lein, J. Phys. B **40**, R135 (2007).
[21] M. Spanner, O. Smirnova, P. B. Corkum, and M. Ivanov, J. Phys. B **37**, L243 (2004).
[22] S. N. Yurchenko, S. Patchkovskii, I. V. Litvinyuk, P. B. Corkum, and G. L. Yudin, Phys. Rev. Lett. **93**, 223003 (2004).
[23] T. Morishita, A. T. Le, Z. Chen, and C. D. Lin, Phys. Rev. Lett. **100**, 013903 (2008).
[24] Z. Chen, A. T. Le, T. Morishita, and C. D. Lin, Phys. Rev. A **79**, 033409 (2009).
[25] H. Stapelfeldt and T. Seideman, Rev. Mod. Phys. **75**, 543 (2003).
[26] S. Lothar, Appl. Spectrosc. **30**, 123 (1976).
[27] P. D. McCaffrey, J. K. Dewhurst, D. W. H. Rankin, R. J. Mawhorter, and S. Sharma, J. Chem. Phys. **128**, 204304 (2008).
[28] S. Hinchley, D. A. Wann, and D. W. H. Rankin, Int. J. Quantum Chem. **101**, 878 (2005).
[29] H. Cohen and U. Fano, Phys. Rev. **150**, 30 (1966).
[30] B. Yang, K. J. Schafer, B. Walker, K. C. Kulander, P. Agostini, and L. F. DiMauro, Phys. Rev. Lett. **71**, 3770 (1993).
[31] M. V. Frolov, N. L. Manakov, T. S. Sarantseva, and A. F. Starace, J. Phys. B **42**, 035601 (2009).
[32] M. V. Frolov, N. L. Manakov, and A. F. Starace, Phys. Rev. A **79**, 033406 (2009).
[33] A. Čerkić, E. Hasović, D. B. Milošević, and W. Becker, Phys. Rev. A **79**, 033413 (2009).
[34] O. I. Tolstikhin, T. Morishita, and S. Watanabe, Phys. Rev. A **81**, 033415 (2010).
[35] D. Ray *et al.*, Phys. Rev. Lett. **100**, 143002 (2008).
[36] M. Okunishi, T. Morishita, G. Prümper, K. Shimada, C. D. Lin, S. Watanabe, and K. Ueda, Phys. Rev. Lett. **100**, 143001 (2008).
[37] S. Micheau, Z. J. Chen, A. T. Le, J. Rauschenberger, M. F. Kling, and C. D. Lin, Phys. Rev. Lett. **102**, 073001 (2009).
[38] X. M. Tong, Z. X. Zhao, and C. D. Lin, Phys. Rev. A **66**, 033402 (2002).
[39] S. F. Zhao, C. Jin, A. T. Le, T. F. Jiang, and C. D. Lin, Phys. Rev. A **81**, 033423 (2010).
[40] D. L. Carroll, FORTRAN genetic algorithm driver, 1999 [http://cuaerospace.com/carroll/ga.html] (accessed in May 2008).
[41] J. Xu, H.-L. Zhou, Z. Chen, and C. D. Lin, Phys. Rev. A **79**, 052508 (2009).
[42] T. Morishita, T. Umegaki, S. Watanabe, and C. D. Lin, J. Phys. Conf. Ser. **194**, 012011 (2009).
[43] D. F. Register, H. Nishimura, and S. Trajmar, J. Phys. B **13**, 1651 (1980).
[44] I. Iga, M. G. Homem, K. T. Mazon, and M.-T. Lee, J. Phys. B **32**, 4373 (1999).
[45] I. Kanik, D. C. McCollum, and J. C. Nickel, J. Phys. B **22**, 1225 (1989).

[46] H. Tanaka, T. Ishikawa, T. Masai, L. Beosten, M. Takekawa, Y. Itikawa, and M. Kimura, Phys. Rev. A **57**, 1798 (1998).
[47] T. Andersen, H. K. Haugen, and H. Hotop, J. Phys. Chem. Ref. Data **28**, 1511 (1999).
[48] L. I. Schiff, *Quantum Mechanics* (McGraw-Hill, New York, 1968), 3rd ed., p. 145.
[49] I. Iga, I. P. Sanches, P. Rawat, M. G. P. Homem, and M.-T. Lee, J. Phys. B **38**, 3477 (2005).
[50] H. S. W. Massey and E. C. Bullard, Proc. Cambridge Philos. Soc. **29**, 511 (1933).
[51] D. Herrmann, K. Jost, J. Kessler, and M. Fink, J. Chem. Phys. **64**, 1 (1976).
[52] I. Iga, I. P. Sanches, E. de Almeida, R. T. Sugohara, L. Rosani, and M.-T. Lee, J. Electron Spectrosc. Relat. Phenom. **155**, 7 (2007).
[53] L. M. Brescansin, I. Iga, and M.-T. Lee, J. Phys. B **37**, 471 (2004).
[54] S. Habershon and A. H. Zewail, ChemPhysChem **7**, 353 (2006).
[55] Z. Zhou and K. D. M. Harris, Chem. Phys. Chem. **10**, 7262 (2008).
[56] J. C. Williamson and A. H. Zewail, J. Phys. Chem. **98**, 2766 (1994).
[57] V. Sreedhara Rao, A. Vijay, and A. K. Chandra, Can. J. Chem. **74**, 1072 (1996).
[58] C. Cornaggia, J. Phys. B **42**, 161002 (2009).
[59] M. Okunishi, R. Itaya, K. Shimada, G. Prümper, K. Ueda, M. Busuladžić, A. Gazibegović-Busuladžić, D. B. Milošević, and W. Becker, J. Phys. B **41**, 201004 (2008).
[60] M. Busuladžić, A. Gazibegović-Busuladžić, D. B. Milošević, and W. Becker, Phys. Rev. Lett. **100**, 203003 (2008).
[61] M. Meckel *et al.*, Science **320**, 1478 (2008).
[62] O. Smirnova, S. Patchkovskii, Y. Mairesse, N. Dudovich, and M. Y. Ivanov, Proc. Natl. Acad. Sci. USA **106**, 16556 (2009).
[63] R. Torres *et al.*, Phys. Rev. A **81**, 051802(R) (2010).